Proceedings of the Seventh International Conference on Creationism.
Pittsburgh, PA: Creation Science Fellowship

NEW MATERIAL MODEL REVEALS INHERENT TENDENCY IN MANTLE MINERALS FOR RUNAWAY MANTLE DYNAMICS

Jesse A. Sherburn, Ph.D., 13 Old Waverly Lane, Vicksburg, MS 39183
John R. Baumgardner, Ph.D., 24515 Novato Place, Ramona, CA 92065
Mark F. Horstemeyer, Ph.D., 1292 Chapel Hill Road, Starkville, MS 39759

KEYWORDS: Genesis Flood, catastrophic plate tectonics, runaway subduction, mantle rheology, computational modeling, solid-state plasticity, material model, internal state variable method

ABSTRACT

In this paper we apply a material model used for years in the engineering community to simulate deformation and failure of metal components to the problem of deformation of silicate minerals in the earth's mantle. Known as the Bammann inelastic internal state variable (BIISV) model, this formulation utilizes not only the current state (e.g., temperature, density, stress) of each material parcel to compute the current deformation rate, but it also carries along features (internal state variables) that describe the parcel's deformational history. This history information allows the model to represent more complex modes of material deformation than models which do not include such information. This study reveals for the first time that a type of solid-state plastic deformation known as dislocation glide may well be the crucial mechanism responsible for buoyancy-driven runaway in the mantle of a planet with a mass and gravity field like that of the earth. To explore the tendency for runaway behavior we applied a 2D Cartesian version of the finite element TERRA mantle dynamics program that includes the BIISV model. We obtain BIISV parameters appropriate for the earth's mantle from experimental measurements of the material properties of the upper mantle rock lherzolite. We find that buoyancy anomalies of plausible size yield spectacular runaway behavior when the dislocation glide mechanism is enabled.

INTRODUCTION

Baumgardner (1986, 1990, 1994a, 1994b, 2003) has argued persuasively that huge volumes of oceanic lithosphere must have been recycled into the mantle during the Genesis Flood. This conclusion is based on the observational evidence that the totality of today's igneous ocean floor is younger than much of the continental fossil-bearing sediment record. This implies not only that all the pre-Flood ocean floor is missing from today's ocean basins but also that the entirety of the current ocean floor has formed by seafloor spreading at a mid-ocean ridge since the Flood itself began. This logically requires that a vast amount of subduction of the older oceanic

lithosphere and the creation of new ocean lithosphere along the mid-ocean ridge system must have accompanied the Flood. As such it must have been a major aspect of the entire cataclysm. This scenario of large amounts of ocean lithosphere subducting into the mantle and being replaced with a new ocean lithosphere along the mid-ocean ridges during the year of the Flood has come to be known as catastrophic plate tectonics. The energy source that drives the process is gravitational potential energy, not only of the cold lithosphere, but also of the hot rock at the core-mantle boundary that rises to replace the cold lithosphere near the earth's surface.

In each of these earlier studies by Baumgardner, a paramount issue has been the mechanism by which the rock in the mantle weakens from the high values (10^{22} Pa-s) it displays today to values many orders of magnitude smaller that could allow lithospheric slabs and rising plumes to traverse the approximately 3000 km thickness of the mantle in the span of only a few weeks. In Baumgardner (1986; 1990), the mechanism of thermal weakening was explored. In Baumgardner (1994a,b) the weakening associated with power-law creep was added. While a tendency toward runaway was demonstrated in the 1994 2D calculation, actual runaway was not achieved. One reason was that the material model simply did not provide sufficient weakening. A second reason was numerically related—the best numerical methods at that point in time were not yet robust enough to cope with the extreme gradients that arise under runaway conditions.

In 2000 W.-S. Yang, whom Baumgardner advised as a graduate student at the University of Illinois, published a numerical method Yang had developed as part of his Ph.D. thesis research that provided the needed robustness (Yang and Baumgardner, 2000). Then in 2003 Baumgardner added a yield criterion into the material model he had described in his 1994 paper. Utilizing Yang's improved numerical method and allowing mantle rock to yield when stress exceeded a specified yield stress value, Baumgardner obtained spectacular runaway behavior (Baumgardner, 2003). The value of yield stress of 75 MPA Baumgardner used was in the range reported by Baumgardner and Yang (1999) that, when applied to the lithosphere, also resulted in self-consistent plates in 3D spherical geometry. That value was also in the range found by Tackley (2000) that, when applied in the lithosphere, gave plate results in 3D Cartesian mantle convections models. The problem was that such a low value of yield stress, while accounting for lithospheric weakening due to water and sediment in subduction zones and melting at mid-ocean ridges, had no actual experimental support for depths below the lithosphere. In other words, the finite element simulations used a material property, the yield stress, which though valid for the lithosphere, could not be justified for the rock of the deeper mantle. This deficiency motivated a search for a material model that would represent the deformational behavior of mantle rock with greater fidelity and include other mechanisms that could lead to weakening.

The work of Horstemeyer (1998) and then Horstemeyer and Baumgardner (2003) represented a first step toward addressing this need. They investigated various weakening mechanisms in the mineral olivine using a variation of the Bammann inelastic internal state variable (BIISV) model. More recently, Sherburn *et al.* (2011a) applied the BIISV to other relevant mantle materials. Sherburn *et al.* (2011b) then implemented the BIISV model in the 2D version of Baumgardner's

TERRA code. The BIISV model is able to represent behavior that the previous power-law formulation could not. Some of the features included in the current ISV model are the ability to include history effects, plasticity, creep, recrystallization, damage accumulation, and texture effects. In this paper we report results from the BIISV model in the framework of TERRA2D code that captures a critical behavior known as dynamic recovery. We find that this more realistic material model does indeed display weakening behavior strong enough to produce runaway motion in the mantle of a planet with the mass and gravity field of the earth.

MODEL DESCRIPTION

Prior to incorporating the BIISV model, TERRA2D had a composite diffusion creep/power-law creep/yield stress material model for the constitutive response of mantle rock. Shortcomings of this type of model are that it does not track material history and it does not capture several important deformation mechanisms of dislocation motion. Dislocations are line-like crystallographic defects that occur within a crystal structure. Plastic deformation of a crystal can involve dislocations gliding or climbing on crystallographic planes. Dislocation glide involves the movement of dislocations along glide planes in the crystalline lattice. In metals dislocation glide plays an important role in manufacturing processes such as rolling, forging, and sheet forming (Deiter, 1986). Dislocation climb also involves motions of dislocations but of a different type and is usually associated with slower deformation. Both mechanisms of glide and climb have been quantified in metals and rocks and have been summarized by Ashby (1972). Kohlstedt and Goetze (1974) and Kirby (1983) provided analyses of the dislocation mechanisms for olivine and other silicates. Another deficiency of the creep/power law model is that it cannot be calibrated to experimental data over a broad strain rate and temperature range.

The BIISV model was introduced into TERRA2D to overcome these shortcomings. It is a history-dependent elastic-viscoplastic material model developed from a unified-creep-plasticity theory that includes strain rate and temperature effects. The internal state variables capture the thermodynamic history state of the material which in turn is linked explicitly to dislocation motion (both glide and climb). The BIISV model was originally developed by Bammann (1990), and its original application was to metallic materials. However, the model can be applied to any polycrystalline solid that deforms via dislocation motion (Horstemeyer, 1998). Higher temperature polycrystalline rocks like the ones that comprise the earth's mantle are well known to deform by motion of dislocations that have both glide and climb mechanisms (Kohlstedt *et al.*, 1995).

The notion of internal state variable (ISV) theory was introduced into thermodynamics by Onsager (1931a, 1931b) and was applied to continuum mechanics by Eckart (1940, 1948). The ISV formulation represents an attempt to capture important stress-strain behavior of a representative volume element without monitoring all of the complex phenomena that occur at the finer scales. In other words, an ISV method seeks in some fashion to average macroscopically the details of the microscopic arrangement. In essence, the complete

microstructure arrangement is unnecessary so long as the macroscale ISV representation is complete (cf., Kroner, 1964). As a result, the ISV representation must be based on physically observable behavior and constrained by the laws of thermodynamics (Coleman and Gurtin, 1967). From the viewpoint of rational thermodynamics, the ISVs provide the additional information necessary for a rational description of the thermodynamic state of the material. From the viewpoint of thermodynamics of irreversible processes (Rice, 1971), the ISVs provide the information required to describe neighboring constrained equilibrium states.

In modeling the deformation associated with dislocations it is common to describe it in terms of hardening and recovery of the material. As dislocations migrate through a crystal in response to stress, their motion can be constrained as they encounter crystal boundaries as well as other dislocations and other crystallographic defects. As dislocation motion is constrained, the strength of the material increases and the material is said to harden. On the other hand, as the density of dislocations increases, they can begin to annihilate one another. This annihilation reduces the strength and weakens the material. This process is referred to as recovery. The hardening-recovery format for modeling plasticity in relation to dislocation behavior was first introduced by Armstrong and Frederick (1966).

The ISVs included in the BIISV model describe the isotropic and kinematic hardening/recovery associated with dislocations. Isotropic hardening represents statically stored dislocations that cause growth in the yield surface volume. Kinematic hardening represents geometrically necessary dislocations that have the general effect of deforming a material's yield surface without changing its volume. In metals this phenomenon of deforming the yield surface is known as the Bauschinger effect. It is unknown at this time how strongly geologic materials might exhibit this effect. Our ISV equations are cast in this hardening-recovery format and can be thought of as the responses to thermodynamic forces arising from kinematic constraints of dislocation nucleation, motion, and trapping. As such, the kinematic and isotropic hardening equations are at the heart of the BIISV model and have been shown to accurately describe a broad range of crystallographic materials in terms of hardening and recovery associated with dislocation glide and climb. In the BIISV model kinematic hardening is expressed in terms of a kinematic hardening tensor $\underline{\alpha}$ which has units of stress (force/area). Isotropic hardening is expressed in terms of an isotropic hardening scalar R that also has units of force/area. The kinematic and isotropic hardening equations in the BIISV model (Bammann *et al*., 1996) expressing the time rate of change of $\underline{\alpha}$ and R, respectively, are

$$\underline{\overset{\nabla}{\alpha}} = h(T)\underline{D}^{in} - \left(\sqrt{\frac{2}{3}} r_d(T)\left\|\underline{D}^{in}\right\| + r_s(T)\right)\|\underline{\alpha}\|\underline{\alpha} \tag{1}$$

$$\dot{R} = \left[H(T)\left\|\underline{D}^{in}\right\| - \left(\sqrt{\frac{2}{3}} R_d(T)\left\|\underline{D}^{in}\right\| + R_s(T) \right) R^2 \right] \tag{2}$$

Here D^{in} is the inelastic strain rate and T is temperature. The quantities h and H are temperature-dependent hardening factors. The leading term on the right hand side of each of these equations represents in a continuum sense the hardening effects of dislocations. The second term describes what is known as recovery and represents the annihilation of dislocations. Recovery is divided into two parts, a dynamic part that depends on strain rate and a static part that does not. The temperature dependent factors r_d and R_d specify the strength of dislocation glide associated with kinematic and isotropic dynamic recovery, respectively. The temperature dependent factors r_s and R_s specify the strength of dislocation climb associated with kinematic and isotropic static recovery, respectively. Note that the dynamic and static recovery terms are weakening terms as they subtract from the work hardening term. The recovery mechanism associated with dislocation glide is different from that associated with dislocation climb. Because recovery associated with dislocation glide typically occurs at a higher rate, it is referred to as dynamic recovery. Recovery associated with dislocation climb, because it typically occurs at a lower rate, is referred to as static recovery. Both mechanisms occur in silicate rocks (Kirby, 1983; Poirier and Vergobbi, 1978) and involve the annihilation of dislocations. Since both mechanisms have been observed we are justified in including dislocation climb and dislocation glide effects. The implications of both of these terms in the context of the mantle will be discussed in the results section.

To apply the BIISV model to the earth we chose to fit the BIISV parameters to experimental data available for a rock type known as lherzolite (Carter and Ave'Lallemant, 1970). Lherzolite was selected because it is a good representative of upper mantle mineralogy. Lherzolite is a fine-grained nearly equiaxed granular rock comprising 60%-70% olivine, 20%-30% enstatite, 5%-10% diopside, and less than 1% spinel. Because the experimental measurements provide constraints only for the isotropic portion of the BIISV model, given by equation (2), we have ignored the kinematic portion, represented by equation (1). Based on how well we are able to fit the experimental data using only the isotropic portion, we feel that this approximation is justifiable and realistic. While Sherburn *et al.* (2011a) included only the static recovery (dislocation climb) term to fit the stress-strain data, both the dynamic recovery and static recovery terms are employed in the current study. The correlation between the BIISV model and the experimental measurements is shown in Figure 1. Notice that the model does an excellent job of matching experimental data over the experimental strain rate and temperature range. (The Appendix provides the actual values for the BIISV constants.)

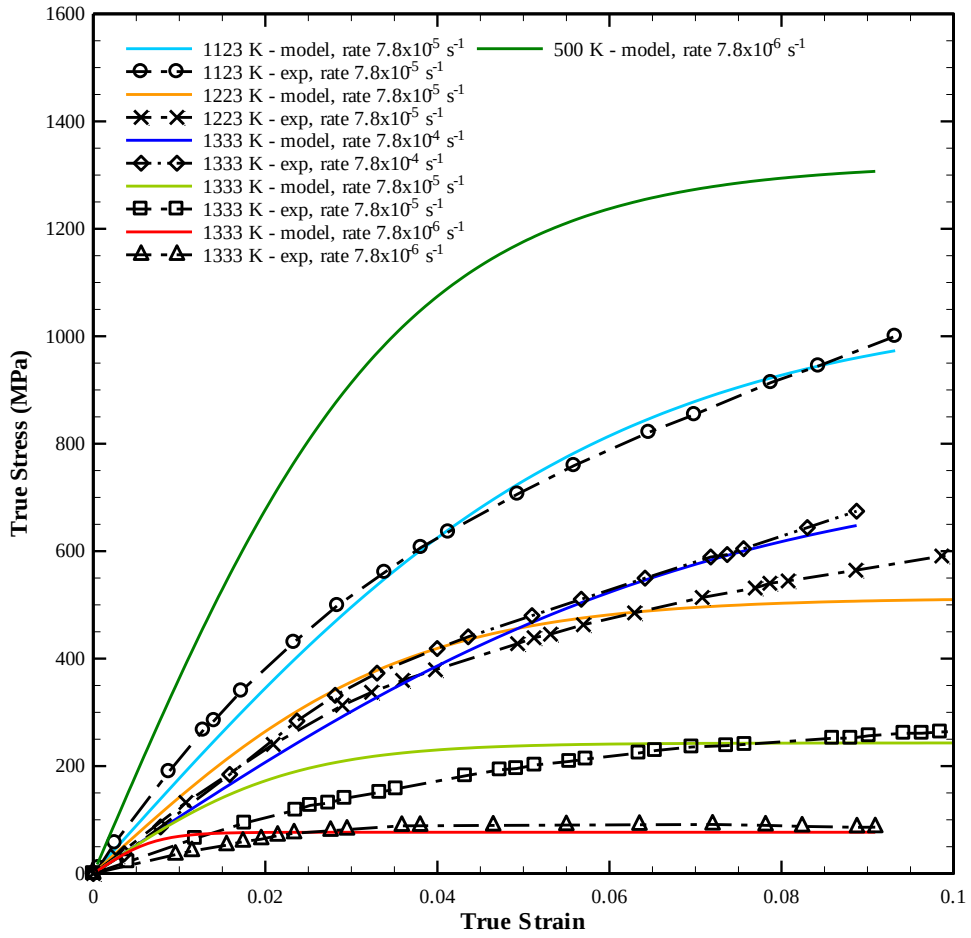

Figure 1. BIISV model correlation to lherzolite experimental data (Carter and Ave'Lallemant, 1970) obtained by Sherburn *et al*. (2011a).

Due to the relative ease of implementation and also its relatively low computational cost, the two-dimensional version of TERRA (TERRA2D), developed by Yang and Baumgardner (2000), was chosen as the framework in which to implement the BIISV model to explore its applicability to geophysical applications. The details of the implementation will not be discussed here but are found in Sherburn *et al.* (2011b).

Of course, a realistic reference temperature distribution for the mantle is required for mantle simulations. We obtain a vertical reference temperature profile by first assuming reasonable values for the temperature jumps across the upper and lower thermal boundary layers of the mantle. We then apply the widely used Birch-Murnaghan equation of state (Birch, 1947), calibrated to the preliminary reference earth model (Dziewonski and Anderson, 1981), to obtain the adiabatic temperature change across the mantle's interior. This reference temperature profile in turn is used to compute the initial viscosity profile from the BIISV model. The lherzolite BIISV parameters, however, are specific to the upper mantle and must be modified slightly for deeper regions of the mantle. For simplicity, we divided the mantle into three zones: upper

mantle, transition zone, and lower mantle. The model constants were adjusted slightly to yield an initial viscosity profile, displayed in Figure 2, which matches viscosity profiles published by Cizkova *et al.* (2012). Currently, experimental limitations restrict laboratory measurements for fitting the BIISV parameters to upper mantle pressures and therefore to upper mantle minerals and rocks (Karato, 2008). When experimental capabilities become available to characterize lower mantle rocks, it will be straightforward to obtain even more realistic BIISV parameters for the deeper mantle using the same procedures as described in Sherburn *et al.* (2011a).

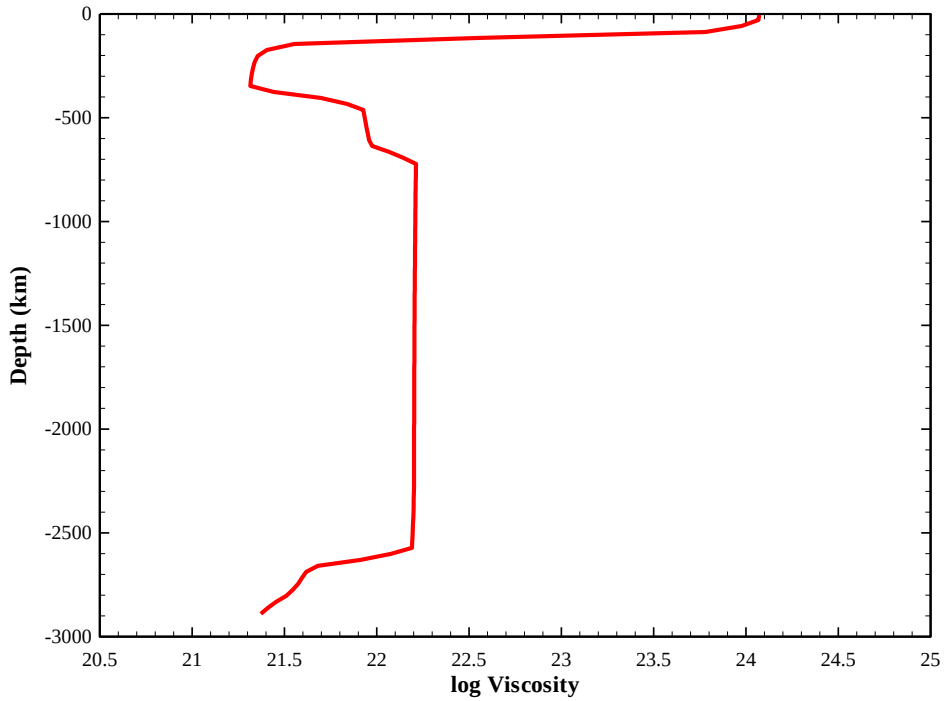

Figure 2. The initial vertical viscosity profile for the TERRA2D calculations. The parameters for the BIISV material model for the different depth zones were adjusted to constrain the profile to match estimates for the present day earth.

Two different simulation cases were constructed to explore possible runaway behavior in the mantle using the BIISV model. The first case (Case 1) the initial condition includes a blob of cold material 300 km wide extending to a depth of 650 km at a temperature of 300 K in the upper mantle and a hot perturbation of similar size in the lower mantle. Buoyancy acting on these density anomalies serves immediately to drive mantle flow. Figure 3 shows the initial temperature distribution and the initial viscosity profile for Case 1. The initial condition for second case (Case 2) includes a much smaller cold blob (100 km wide and 650 km deep) in the upper mantle and a hot blob of similar size in the lower mantle, as displayed in Figure 4. Also, two different BIISV settings (one allowing both static and dynamic recovery and the other allowing static recovery alone) were applied for both cases. Results are described in the next section.

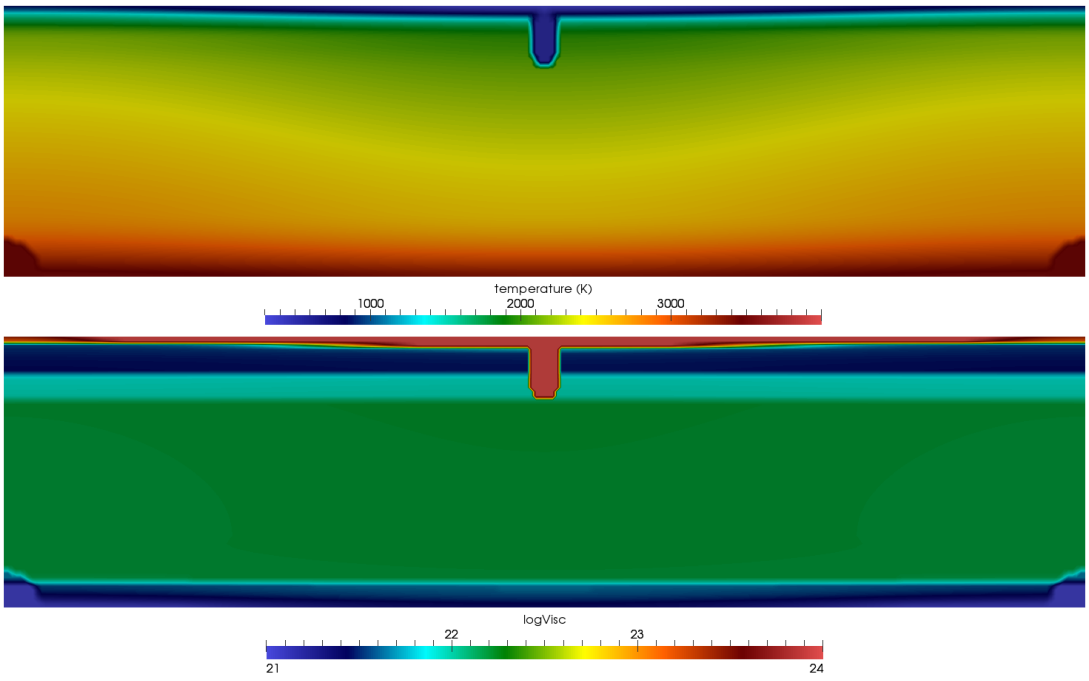

Figure 3. The initial temperature and viscosity fields for the Case 1 simulation with large initial temperature perturbations.

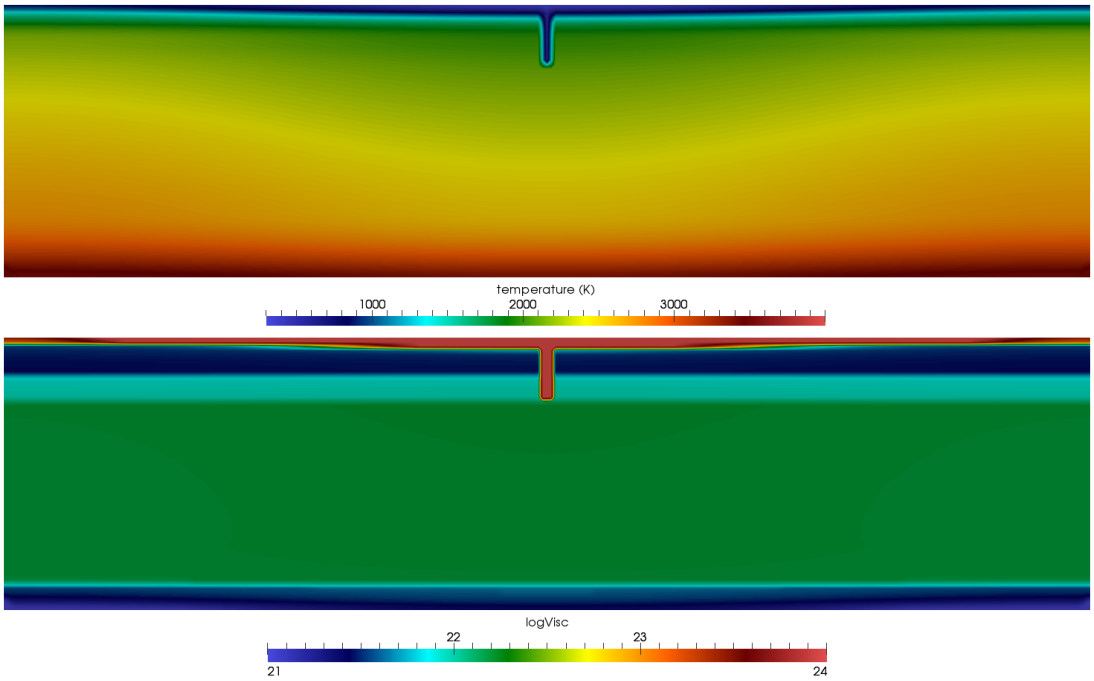

Figure 4. Initial viscosity and temperature fields for Case 2 with smaller initial temperature perturbations.

RESULTS/DISCUSSION

Case 1 with both dynamic and static recovery terms included gave spectacular runaway behavior. Figure 5 displays the state of the mantle after two days. Deformation of the mantle by the sinking of the cold blob, driven by its gravitational potential energy, has dramatically lowered the mantle viscosity and is enabling the blob to plunge downward at 1–2 m/s. Note that viscosity has dropped by nine orders of magnitude (a billion fold) and more in much of the mantle relative to its initial viscosity state of Figure 3. Also noteworthy in the viscosity plot of Figure 5 are large diagonal low viscosity zones that cross from the hot blobs in the lower mantle to the colder blob in the upper mantle. These low viscosity bands (LVBs) behave much like global shear bands that facilitate the cold blob's downward plunge. After 45 days the cold blob reaches the bottom of the mantle as shown in Figure 6. The original LVBs have followed the path of the plunging blob and some new LVBs emanated from the ascending hot blobs. The mantle velocities achieved peak values around day 45. These new LVBs enable the hot blobs to run away upward and reach the upper mantle also around day 45.

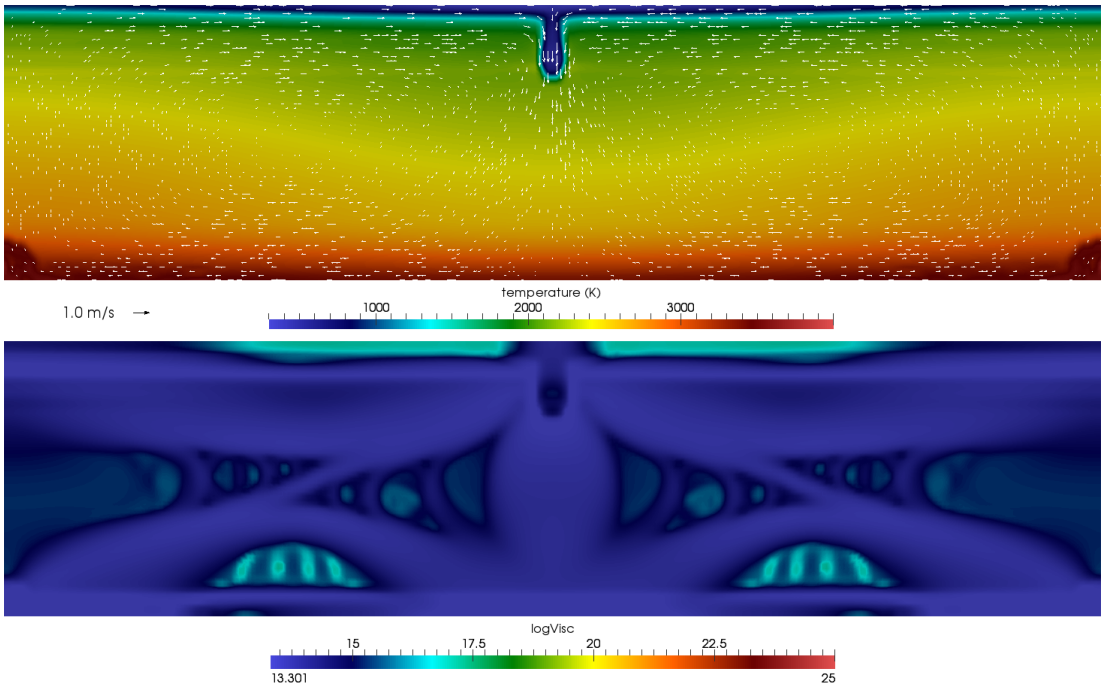

Figure 5. Day 2 after the onset of runaway for Case 1. Notice the low viscosity band (LVB) formed diagonally across the lower mantle.

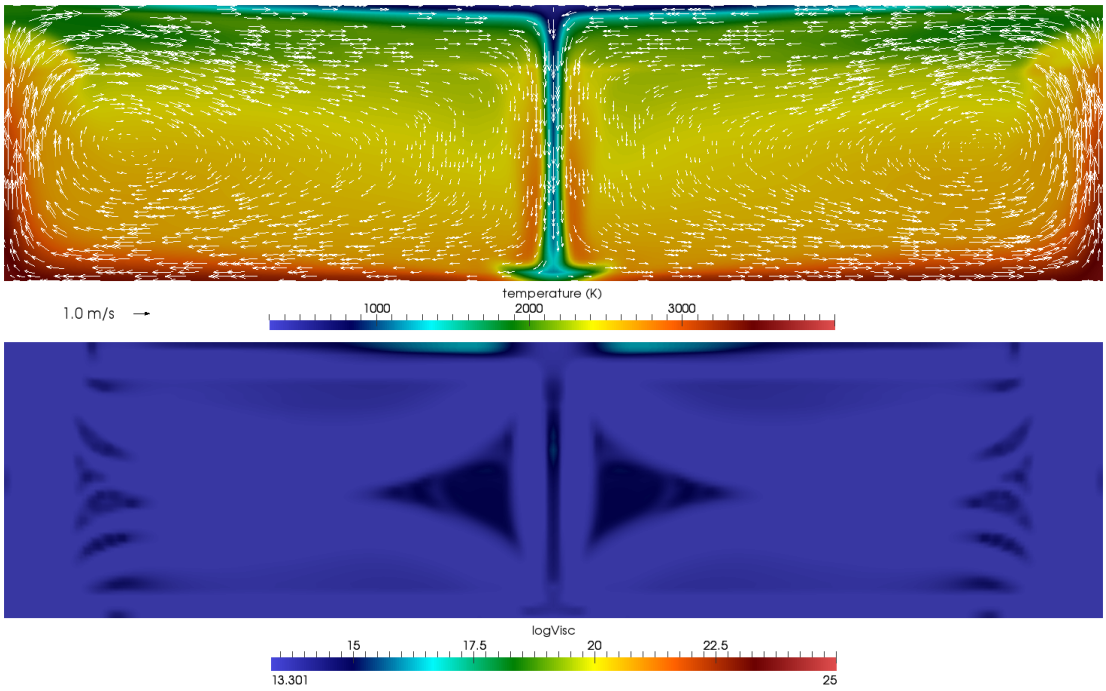

Figure 6. Day 45 after the onset of runaway for Case 1. The cold blob has reached the bottom of the mantle and the hot blob has risen into the upper mantle.

As the simulation continues, the hot blobs push the remainder of the colder thermal boundary layer toward the center as shown in Figure 7 at day 80. Notice in Figure 7 that the earlier diagonal LVBs that enabled runaway to progress have disappeared. However, some lingering vertical LVBs remain along the paths where the original cold and hot blob traversed the mantle. These persistent LVBs allowed the cold upper boundary layer to continue to deform and move. Also noteworthy in Figure 7 is that much of the lower mantle has begun to strengthen and to resist flow. We continued the simulation to a few thousand years to see how much of the cold thermal boundary layer would be transported to the base of the mantle. As shown in Figure 8, the entire cold boundary layer is carried to the bottom of the mantle. Also in Figure 8 one observes that the lower mantle viscosities have risen to values near 10^{22} Pa-s, which is close to the current estimate as displayed in Figure 2 for the initial state of the mantle.

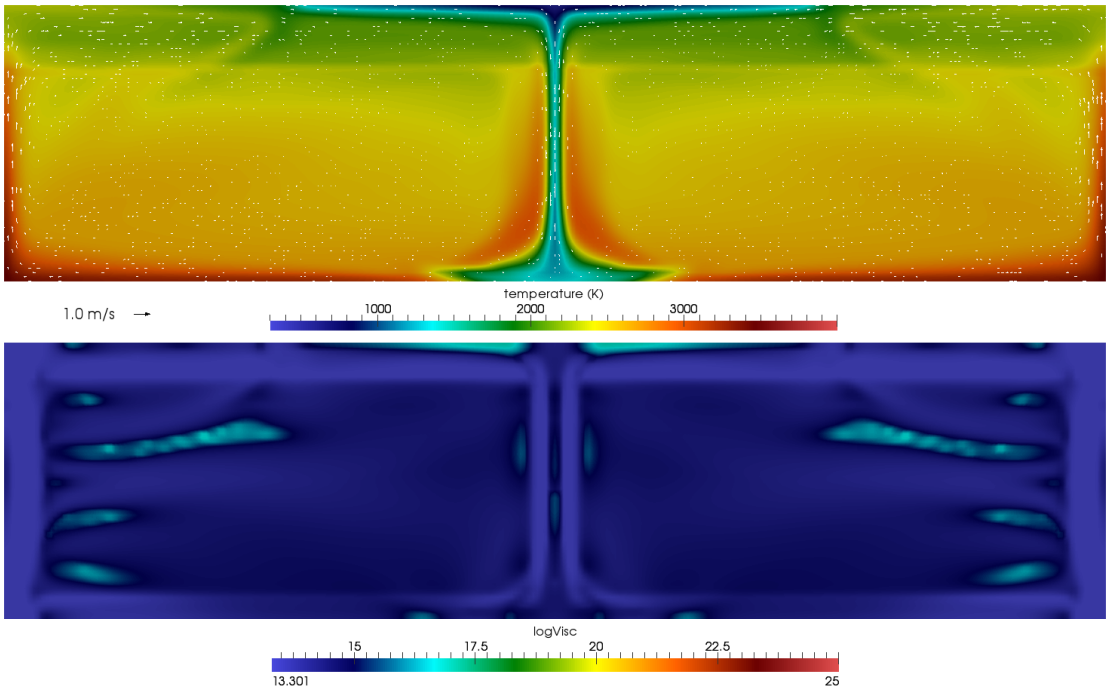

Figure 7. Day 80 after the onset of runaway for Case 1. The cold upper boundary layer continues to flow downward into the mantle. It is pushed laterally by the hotter material that has risen from below. Also notice the lower mantle is beginning to increase in strength in the areas away from the active upward and downward flow.

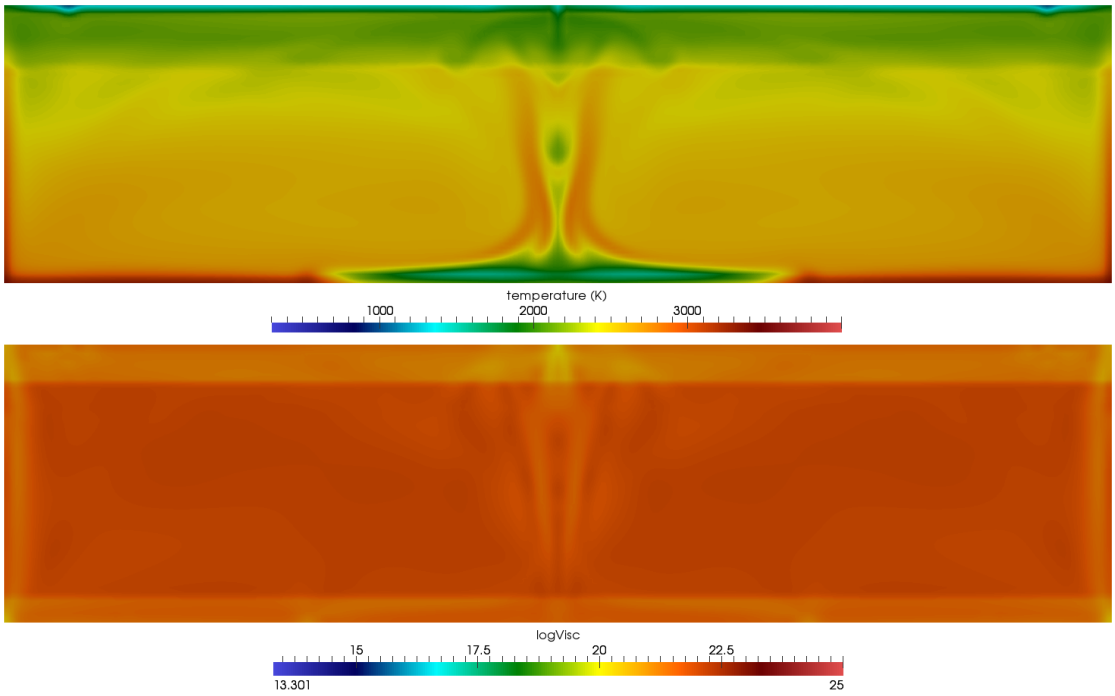

Figure 8. The end of the Case 1 simulation. The cold boundary layer has been completely transported to the bottom boundary, and the mantle has returned to near its original viscosity structure.

Interestingly, the version of Case 1 that included only the static recovery term did not yield runaway but instead remained in equilibrium over the entire period of simulation. Hence, the two different versions of Case 1 argue that dynamic recovery is crucial to runaway behavior. This suggests that it is dislocation glide in mantle minerals which is responsible for the weakening that leads to runaway.

However, even with the dynamic recovery term included, Case 2 displayed no hint of runaway. Figure 9 is a snapshot from Case 2 at around 1.25 million years simulation time. The smaller temperature perturbations were not strong enough to drive this case into the runaway regime. The final viscosity field closely resembles the initial one. Figure 10 shows the vertical velocity profile at 1.25 million years simulation time through the thickness of the mantle. Notice that the velocities are on the order of a few cm/yr which is similar to what is inferred for today's mantle. The surface velocities at this same point in time are shown in Figure 11. These are also on the same order as present plate velocities as measured by GPS methods (Larson et al., 1997).

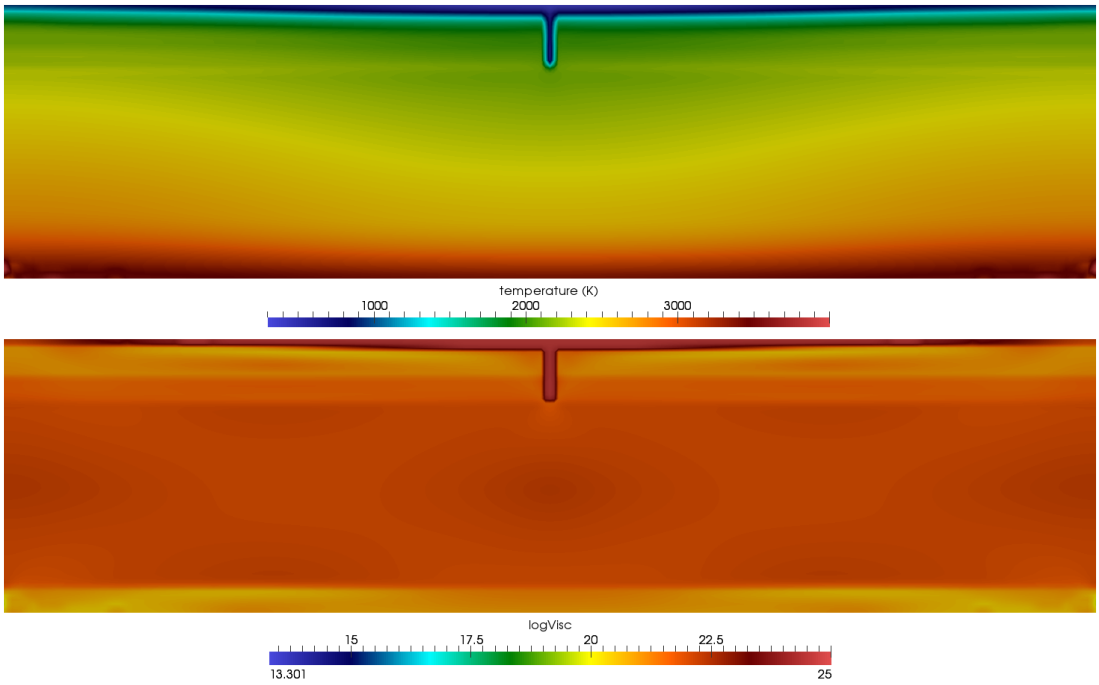

Figure 9. The temperature snapshot after 1.25 million years of simulation time for Case 2. The cold blob does not have enough gravitational potential energy to run away. Notice the viscosity distribution remains in the range of present day estimates.

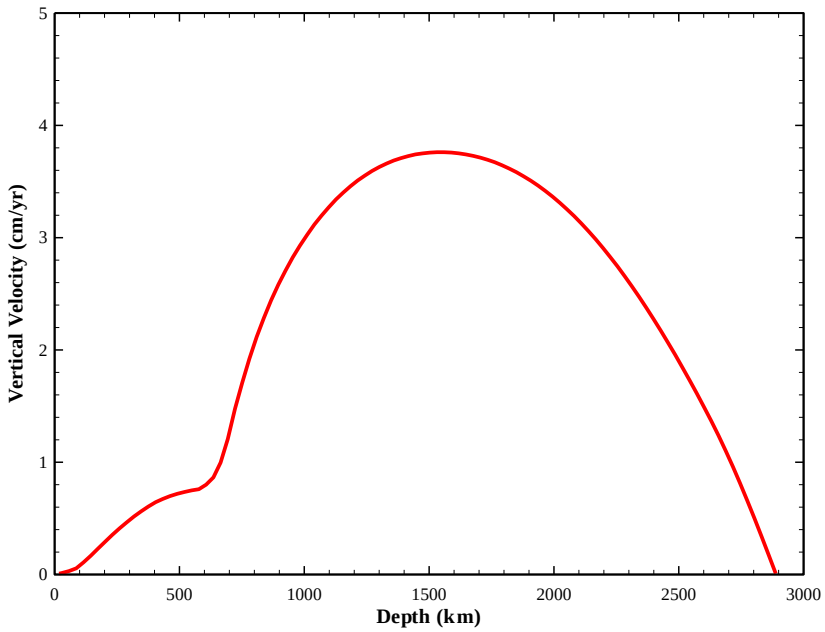

Figure 10. The vertical velocity profile through the thickness of the mantle for Case 2 at 1.25 million years simulation time.

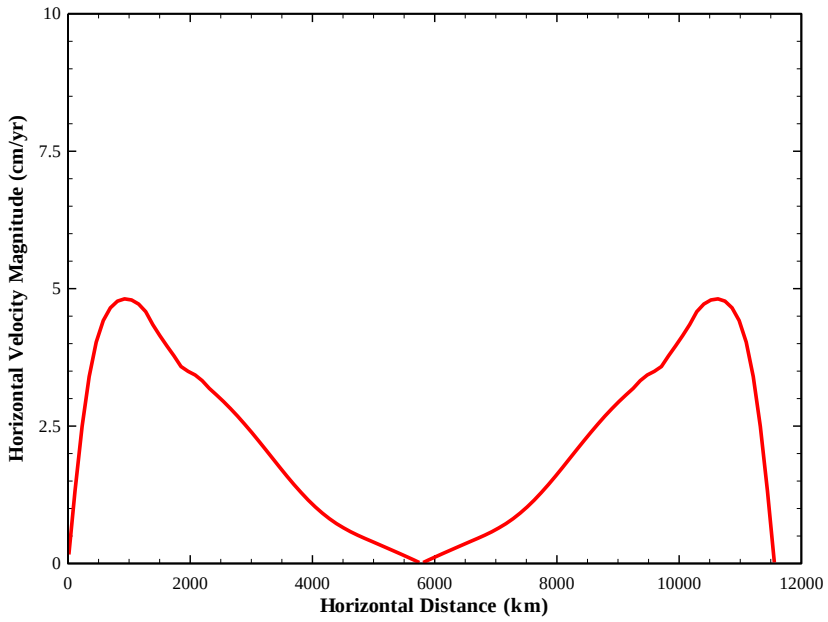

Figure 11. The surface velocity magnitude profile for Case 2 at 1.25 million years simulation time.

When dynamic recovery is allowed, what is it that allows runaway to occur in Case 1 but not in Case 2? The answer obviously involves the size of the initial thermal perturbations and the magnitudes of the resulting shear stress. The higher level of shear stress in Case 1 allows the

dynamic recovery term in the BIISV material model to dominate the influence of the hardening term and results in net weakening. By contrast, the lower shear stress level in Case 2 allows the hardening term to dominate, and the material remains strong. The implication is that there is a threshold of shear stress required for the dynamic recovery to dominate. Future studies are planned to characterize this threshold in more detail.

CONCLUSIONS

The Biblical account in Genesis implies the Flood was a global catastrophe that unfolded in the span of a single year. In this study we find that deformational physics inherent to the BIISV model can result in a runaway mantle overturn within a few months' time for plausible initial conditions. The essential aspect of the BIISV model seems to be the dynamic recovery (dislocation glide) term in hardening/recovery treatment of the plastic flow. When the mantle density anomalies are sufficiently large, the resulting stresses become sufficiently high for this dynamic recovery term to cause weakening to the point of runaway. More experimental data on the deformation properties of mantle rocks would be of considerable value in constraining more accurately the true magnitude of this dislocation glide effect.

REFERENCES

Ashby, M.F.,(1972).A First Report on Deformation Mechanism Maps *Acta Metall*, Vol. 20, Issue 7, 887-897.

Armstrong, P.J. and Frederick, C.O. (1966). A mathematical representation of the multiaxial Bauschinger effect. *CEGB Report RD/B/N*, p. 731.

Bammann, D. J. (1990). Modeling temperature and strain rate dependent large deformations of metals. *Appl. Mech. Rev*., *1*, 312-318.

Bammann, D. J., Chiesa, M. L., and Johnson, G. C. (1996), Modeling large deformation and failure in manufacturing processes. In T. Tatsumi, E. Watanabe, and T. Kambe (Eds.), *Proceedings of the XIXth International Congress of Theoretical and Applied Mechanics*. Kyoto, Japan: Elsevier.

Baumgardner, J. R. (1986). Numerical simulation of the large-scale tectonic changes accompanying the Flood. In R. E. Walsh, C. L. Brooks, and R. S. Crowell (Eds.), *Proceedings of the First International Conference on Creationism* (Vol. 2, pp. 17–28). Pittsburgh, Pennsylvania: Creation Science Fellowship.

Baumgardner, J. R. (1990). 3-D finite element simulation of the global tectonic changes accompanying Noah's Flood. In R. E. Walsh and C. L. Brooks (Eds.), *Proceedings of the Second International Conference on Creationism* (Vol. 2, pp. 35–45). Pittsburgh, Pennsylvania: Creation Science Fellowship.

Baumgardner, J. R. (1994a), Computer modeling of the large-scale tectonics associated with the Genesis Flood. In R. E. Walsh (Ed.), *Proceedings of the Third International Conference on Creationism* (Vol. 2, pp. 48–62). Pittsburgh, Pennsylvania: Creation Science Fellowship.

Baumgardner, J.R. (1994b). Runaway subduction as the driving mechanism for the Genesis Flood. In R. E. Walsh (Ed.), *Proceedings of the Third International Conference on Creationism*, (Vol. 2, pp. 63–86). Pittsburgh, Pennsylvania: Creation Science Fellowship.

Baumgardner, J. R. (2003). Catastrophic Plate Tectonics: The Physics behind the Genesis Flood. In R. L. Ivey Jr. (Ed.), *Proceedings of the Fifth International Conference on Creationism*, (pp. 113-126). Pittsburgh, Pennsylvania: Creation Science Fellowship.

Baumgardner, J.R., and Yang, W.-S. (1999), Earthlike mantle convection from relatively simple rheology (abstract). *Eos, Trans. Am. Geophys. Union, 80, (1999 Fall Meeting Supplement)*, F26.

Carter, N.L., and Ave Lallemant, H.G. (1970). High temperature flow of dunite and perodidite, *Geol. Soc. Am. Bull.*, 81, 2181-2202.

Cizkova, H., van den Berg, A. P., Spakman, W., and Matyska, C. (2012). The viscosity of Earth's lower mantle inferred from sinking speed of subducted lithosphere. *Phys. Earth Plant. Inter.*, http://dx.doi.org/10.1016/j.pepi.2012.02.010

Coleman, B.D., and Gurtin, M.E. (1967). Thermodynamics with internal state variables, *J. Chem. Phys.*, 47, 597-613.

Dieter, G.E. (1986). *Mechanical Metallurgy*, Third Edition, McGraw-Hill, Inc., New York.

Dziewonski, A.M., and Anderson, D. L. (1981). Preliminary reference Earth model. *Phys. Earth Planet Int.* 25, 297-356.

Eckart, C. (1940). Thermodynamics of irreversible processes, I. the simple fluid. *Phys. Rev.*, 58, 267-269.

Eckart, C. (1948). Theory of elasticity and anelasticity. *Phys. Rev.*, 73, 373-382.

Horstemeyer, M.F. (1998). An internal state variable model for geomaterials. In R. E. Walsh (Ed.) *Proceedings of the Fourth International Conference on Creationism*. Pittsburgh, Pennsylvania: Creation Science Fellowship.

Horstemeyer, M.F., and Baumgardner, J.R. (2003), Use of history dependent material models for simulating geophysical events related to the Bible. In R. E. Walsh (Ed.) Proceedings of the Fifth International Conference on Creationism (pp. 303-314). Pittsburgh, Pennsylvania: Creation Science Fellowship.

Karato, S. (2008). *Deformation of Earth Materials: An Introduction to the Rheology of Solid Earth.* Cambridge University Press, pp 474.

Kirby, S.H. (1983). Rheology of the lithosphere, *Reviews Geophys. Space Phys*., *21*, 1458-1487.

Kohlstedt, D. L., Evans, B., and Mackwell, S. J. (1995). Strength of the lithosphere: Constraints imposed by laboratory experiments. *Journal of Geophysical Research, 100,* B9, 17587-17602.

Kohlstedt, D.L. and Goetze, C. (1974). Low-Stress High-Temperature Creep in Olivine Single Crystals. *J. Geophysical Research*, Vol. 79, No. 14, 2045-2051.

Kroner, E. (1964). *Course 3: Continuum Theory of Defects*. Institute fur Theoretische und Angewandte Physik der Universitat Stuttgart und Max Planck Institut fur Metallforschung, Stuttgart, Germany.

Larson, K. M., Freymueller, J. T., and Philipsen, S. (1997). Global plate velocities from the Global Positioning System. *Journal of Geophysical Research, 102,* B5, 9961-9981.

Onsager, L. (1931a). Reciprocal relations in irreversible processes, I. *Phys. Rev.*, 37, 405-426.

Onsager, L. (1931b). Reciprocal relations in irreversible processes, II. *Phys. Rev.*, 38, 2265-2279.

Poirier, J. P., and Vergobbi, B. (1978). Splitting of dislocations in olivine, cross-slip-controlled creep and mantle rheology. *Phys. Earth Planet Int.*, 16, 370-378.

Rice, J. R. (1971). Inelastic constitutive relations for solids: an internal-variable theory and its application to metal plasticity. *J. Mech. Phys. Solids*, 9, 433-455.

Sherburn, J. A., Horstemeyer, M. F., Bammann, D. J., and Baumgardner, J. R. (2011a), Application of the Bammann Inelasticity Internal State Variable Constitutive Model to Geological Materials. *Geophysical Journal International*, 184, 3, 1023-1036. doi: 10.1111/j.1365-246X.2010.04917.x

Sherburn, J. A., Horstemeyer, M. F., Bammann, D. J., and Baumgardner, J. R. (2011b). Two-dimensional mantle convection simulations using an internal state variable model: the role of a history dependent rheology on mantle convection. *Geophysical Journal International*, 186, 3, 945-962. doi: 10.1111/j.1365-246X.2011.05095.x

Tackley, P.J. (2000). Self-consistent generation of tectonic plates in time-dependent, three-dimensional mantle convection simulations: 1. Pseudoplastic yielding. *Geochemistry, Geophysics, Geosystems, 1*, paper number 2000GC000036.

Yang, W.-S., and Baumgardner, J.R. (2000). A matrix-dependent transfer multigrid method for strongly variable viscosity infinite Prandtl number thermal convection. *Geophysical and Astrophysical Fluid Dynamics, 92*, 151-195.

APPENDIX

The constants for lherzolite that were used in this study for the upper mantle are shown in Table 1. All of the constants except C3, C4, C13, C19, and C20 were fit using the procedure outlined in Sherburn *et al.* (2011a). It was found that the constants used in that study did not extrapolate to coldest temperatures (< 1000 K) and the highest temperatures (> 2800 K) required in the current study. The stresses predicted were too high for the colder temperatures, and some additional calibration was necessary to give realistic response over the large temperature range. The constants C3, C4, C19, and C20 were therefore adjusted to give the viscosity profile shown in Figure 4. The constant C13 was added because it constrained the high saturation stresses at the colder temperatures. In Figure 1 the 500 K model response would have been substantially higher (around 4 GPa) if the C13 constant had not been included. The C13 constant in essence limits the maximum stresses that can occur at the colder temperatures.

Table 1. BIISV constants used in the current study for lherzolite.

Constant	Lherzolite Experimental Fit
C1 (MPa)	1.0×10^{-5}
C2 (K)	0.0
C3 (MPa)	10.0
C4 (K)	1000.0
C5 (s^{-1})	1.0×10^{-5}
C6 (K)	0.0
C13(MPa^{-1})	0.05
C14(K)	0.0
C15 (MPa)	1.03×10^{5}
C16 (MPa K^{-1})	65.8
C17 (s MPa^{-1})	4.15
C18 (K)	1.63×10^{4}
C19 (K^{-1})	0.00251
C20 (K)	3200